Supporting Information

Cobalt, iron co-incorporated $Ni(OH)_2$ multiphase for superior multifunctional electrocatalytic oxidation

Pin Hao,‡[a]* Ruirui Xu,‡[a] Qian Wang,[a] Zhenhuan Zhao,[b] Houguang Wen,[a] Junfeng Xie,[a] Fengcai Lei,[a] Guanwei Cui,[a] and Bo Tang[a]*

Experimental

Synthesis of Co, Fe co-incorporated $Ni(OH)_2$ multiphase on carbon cloths (Co Fe:$Ni(OH)_2$ MP/CC)

The catalysts with different molar ratios of Co, Fe and Ni were synthesized in two steps: electrochemical deposition and followed by a hydrothermal process. Firstly, the electro-deposition process was carried out by setting up a three-electrode system, which was performed at -1.0 V (vs SCE) for 5 min in a 100 mL salt solution involving 2 mM $Co(NO_3)_2 \cdot 6H_2O$, 4 mM $Fe(NO_3)_3 \cdot 9H_2O$ and 10 mM $Ni(NO_3)_2 \cdot 6H_2O$. Carbon cloths (denoted as CC, 1 × 4 cm^2) was employed as working electrode, while platinum plate and calomel electrode were used as counter electrode and reference electrode, respectively. After deposition, the sample was washed by deionized (DI) water and ethanol, and dried in the vacuum oven for a night to obtain the Co-Fe-Ni precursor (named as Co-Fe-Ni/CC). Secondly, one piece of above Co-Fe-Ni/CC precursor was placed into a 40 mL clear aqueous solution which was prepared in advance by dissolving 6 mmol dicyandiamide and stirring for 30 min. Then the solution was poured into a 50 mL Teflon-lined stainless steel autoclave to heat at 100 °C for 8 h. After cooling to the room temperature naturally, the sample was removed from solution and cleaned by DI water and ethanol. After drying, the Co, Fe co-incorporated $Ni(OH)_2$ multiphase on carbon cloths (Co Fe:$Ni(OH)_2$ MP/CC, abbreviated simply as CFN MP/CC 2:4:10) were prepared. Other molar ratios of Co, Fe and Ni were synthesized by the same process but different concentrations of cobalt ions and iron ions in the solution during electrochemical deposition process.(0 mM $Co(NO_3)_2 \cdot 6H_2O$, 0 mM $Fe(NO_3)_3 \cdot 9H_2O$ and 10 mM $Ni(NO_3)_2 \cdot 6H_2O$, 0 mM $Co(NO_3)_2 \cdot 6H_2O$, 4 mM $Fe(NO_3)_3 \cdot 9H_2O$ and 10 mM $Ni(NO_3)_2 \cdot 6H_2O$, 1 mM $Co(NO_3)_2 \cdot 6H_2O$, 4 mM $Fe(NO_3)_3 \cdot 9H_2O$ and 10 mM $Ni(NO_3)_2 \cdot 6H_2O$, 3 mM $Co(NO_3)_2 \cdot 6H_2O$, 4 mM $Fe(NO_3)_3 \cdot 9H_2O$ and 10 mM $Ni(NO_3)_2 \cdot 6H_2O$, denoted as β-$Ni(OH)_2$/CC, FN MP/CC 4:10, CFN MP/CC 1:4:10 and CFN MP/CC 3:4:10, respectively.)

Synthesis of α-$Ni(OH)_2$/β-$Ni(OH)_2$ nanosheets and Co incorporated α-$Ni(OH)_2$/β-$Ni(OH)_2$ nanosheets on CC

The Co incorporated α-$Ni(OH)_2$/β-$Ni(OH)_2$ nanosheets grown on CC were prepared through the chemical bath deposition method. Typically, the substrate of CC was placed into a 45 mL aqueous solution containing 5.26 g

$NiSO_4 \cdot 6H_2O$, 0.1 g $Co(NO_3)_2 \cdot 6H_2O$ and 1 g $K_2S_2O_8$. Then, the solution was stirred for several minutes with the addition of 6 mL $NH_3 \cdot H_2O$ (25-28 wt%) drop by drop. After standing the above mixture at room temperature for 2 h, the coated CC was taken out and rinsed with DI water, and then dried in air to obtain Co incorporated α-$Ni(OH)_2$/β-$Ni(OH)_2$ nanosheets (named as CN MP/CC). The α-$Ni(OH)_2$/β-$Ni(OH)_2$ sample (denoted as α/β $Ni(OH)_2$/CC) was synthesized by the same process without the addition of $Co(NO_3)_2 \cdot 6H_2O$.

Synthesis of α-$Ni(OH)_2$ nanosheets on CC

In a typical synthesis, one piece of CC was placed into a 100 mL Teflon-lined stainless-steel autoclave containing 0.6 mmol $Ni(NO_3)_2 \cdot 6H_2O$ and 1.6 mmol urea in 90 mL DI water. Then, the autoclave was sealed and heated at 120 ^{o}C for 12 h. After washing with DI water and drying in vacuum, α-$Ni(OH)_2$ nanosheets on CC were obtained (represented as α-$Ni(OH)_2$/CC).

Structural Characterization

The phase of catalysts was detected by X-ray powder diffraction (XRD) using a Philips X'Pert Pro Super diffractometer with Cu Kα radiation (λ = 1.54178 Å). Since the electrodeposition time is only 5 min, the deposited layer on CC is so thin that the characteristic peaks of $Ni(OH)_2$ are completely covered by the diffraction peaks of carbon. So in order to eliminate the interference of carbon, the sample was put in the DI water with ultrasonic treatment for 10 min, and then dropped the ultrasonic water on a glass slide and dried in an oven. Then we repeated the drop operation on the slide for five times and used the obtained slide to investigate the phase of catalysts using XRD measurement. Field-emission scanning electron microscope (FE-SEM, Hitachi SU8010A) was used to characterize the morphology of samples. High-resolution transmission electron microscopy (HRTEM, JEOLJEM2100F) was employed to study the detailed microstructure of catalysts. The atomic force microscopy (AFM) was conducted on a Cypher VRS AFM equipment (Oxford Instruments) to measure the thickness of nanosheets. The compositional information of the samples was recorded on X-ray photoelectron spectroscopy (XPS, Thermo Scientific ESCLAB250Xi). X-ray spectroscopy (EDX) was used to investigate the element distribution. The molar ratios of Co, Fe and Ni were investigated using the inductively coupled plasma optical emission spectroscope (ICP-OES, Perkin Elmer Optima 7300DV).

Electrocatalytic measurements

A three-electrode system was set up to test the electrocatalytic performance of catalysts. The potential we measured should be converted to a reversible hydrogen electrode (RHE) according to the equation of $E_{vs\ RHE} = E_{vs\ Hg/HgO} + E^{o}_{Hg/HgO} + 0.059pH$. In this work, all potentials are referred to RHE except as specifically indicated. The as-prepared catalysts were applied as the working electrode without binder, while the Hg/HgO electrode and the platinum gauze (2 × 2 cm^2, 60 meshes) were employed as the reference electrode and the counter electrode, respectively. The electrolytes for the OER, UOR and electrochemical organic oxidation (EOO) are 1 M KOH solution, 1 M

KOH with 0.33 M urea, 1 M KOH with 100 mM organic small molecules, respectively. Linear sweep voltammetry (LSV) with scan rates of 2 mV s^{-1}, cyclic voltammetry (CV) with the scan range from 10-100 mV s^{-1} and electrochemical impedance spectroscopy (EIS) were performed at 1.53 V during the frequencies from 0.01 Hz to 100 kHz without IR correction on the electrochemical workstation (CHI660E). The chronoamperometry measurement was conducted at 1.53 V for 20 h. To analyze the products of EOO in 1.0 M KOH with 100 mM BA at 1.43 V vs. RHE for 24 h, 500 μL of the electrolyte solution with 500 μL ethyl acetate was periodically collected during the EOO reaction. The products were analyzed by GC (GC-2010 Plus, SHIMADZU CORPORATION) to calculate the conversion of benzyl alcohol and selectivity of benzoic acid and benzaldehyde. The benzyl alcohol conversion (%) and the selectivity (%) of the oxidation products, and the faradaic efficiency were calculated using the following equations:

$$Conversion\ of\ BA = \frac{moles\ of\ BA\ reacted}{initial\ moles\ of\ BA} * 100\%$$

$$Selectivity\ of\ oxidation\ products = \frac{moles\ of\ oxidation\ products}{moles\ of\ BA\ reacted} * 100\%$$

$$Faraday\ efficiency = \frac{m * n * F}{I * t} * 100\%$$

Where m is the number of moles of the product, n is the number of electrons obtained from the reactant to the product, F is Faraday constant (96485 C mol^{-1}), I is the current, and t is the time.

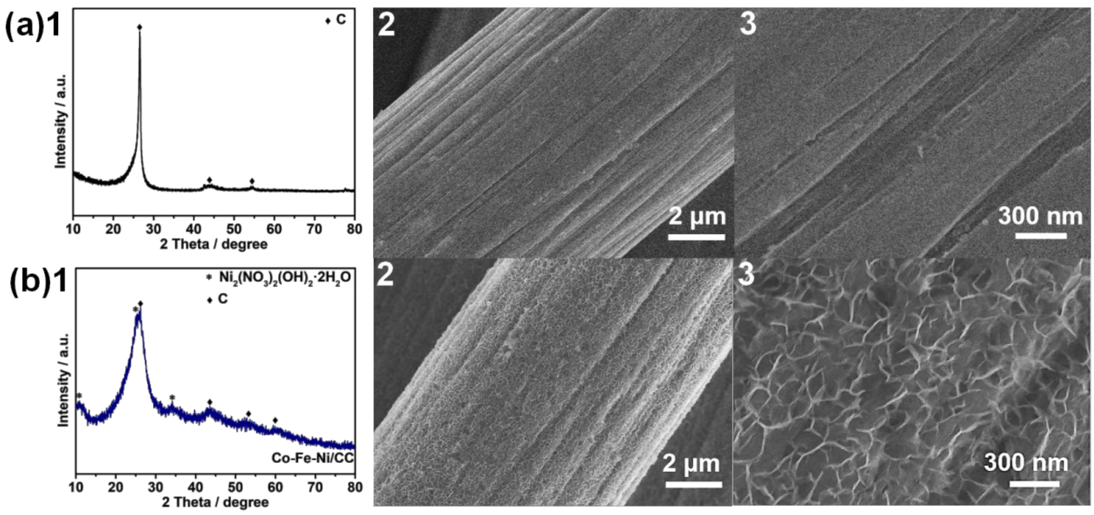

Fig.S1 Phase and morphological characterization of (a) pristine carbon cloths (CC) and (b) Co-Fe-Ni precursors on CC: (1) XRD patterns, (2, 3) SEM images.

The XRD pattern identifies the $Ni_2(NO_3)_2(OH)_2 \cdot 2H_2O$ (JCPDS Card No. 27-0952) phase of Co-Fe-Ni precursor. Note: The diffraction peaks intensity of carbon is so strong that the characteristic peaks of Co-Fe-Ni precursor can't be observed. In order to obtain the phase information of Co-Fe-Ni precursor, the XRD measurement was conducted using the sample which was electrodeposited for 20 min.

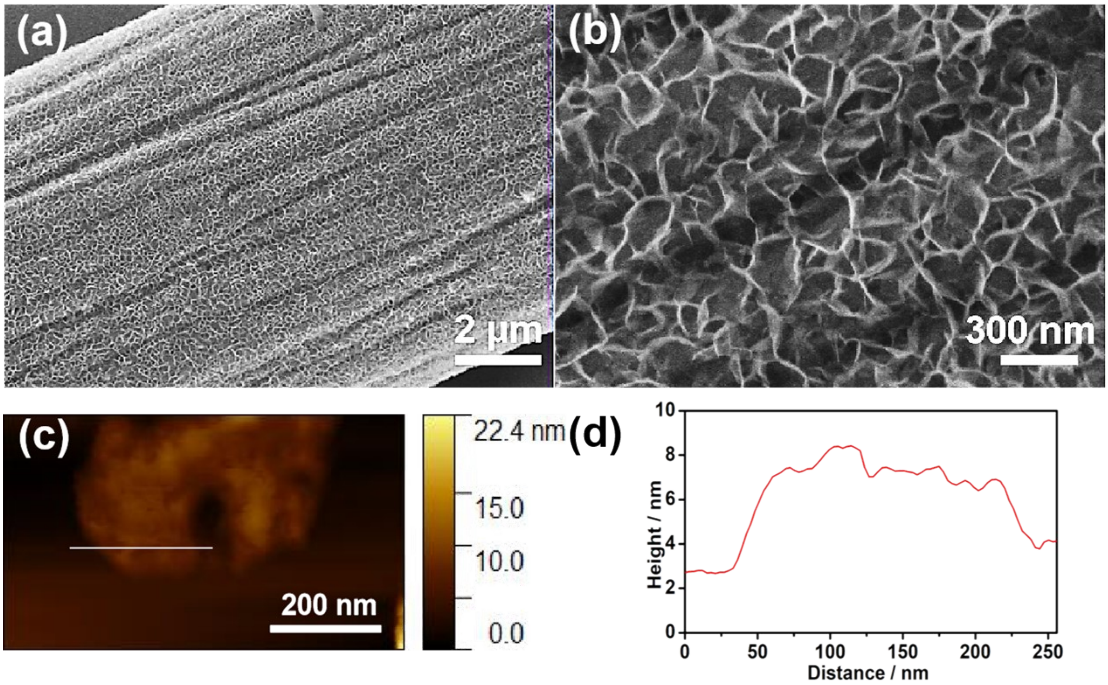

Fig.S2 Morphological information of CFN MP/CC 2:4:10: (a, b) SEM images, (c) AFM image and (d) the corresponding height profile.

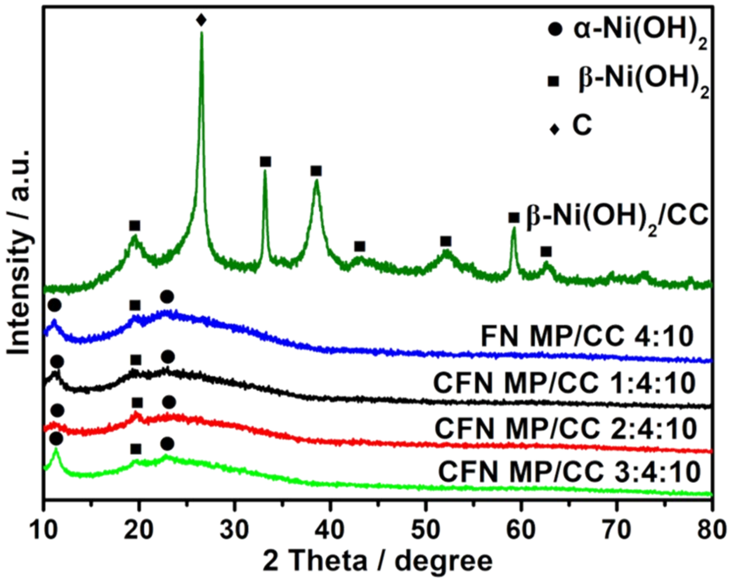

Fig.S3 XRD patterns of the prepared catalysts.

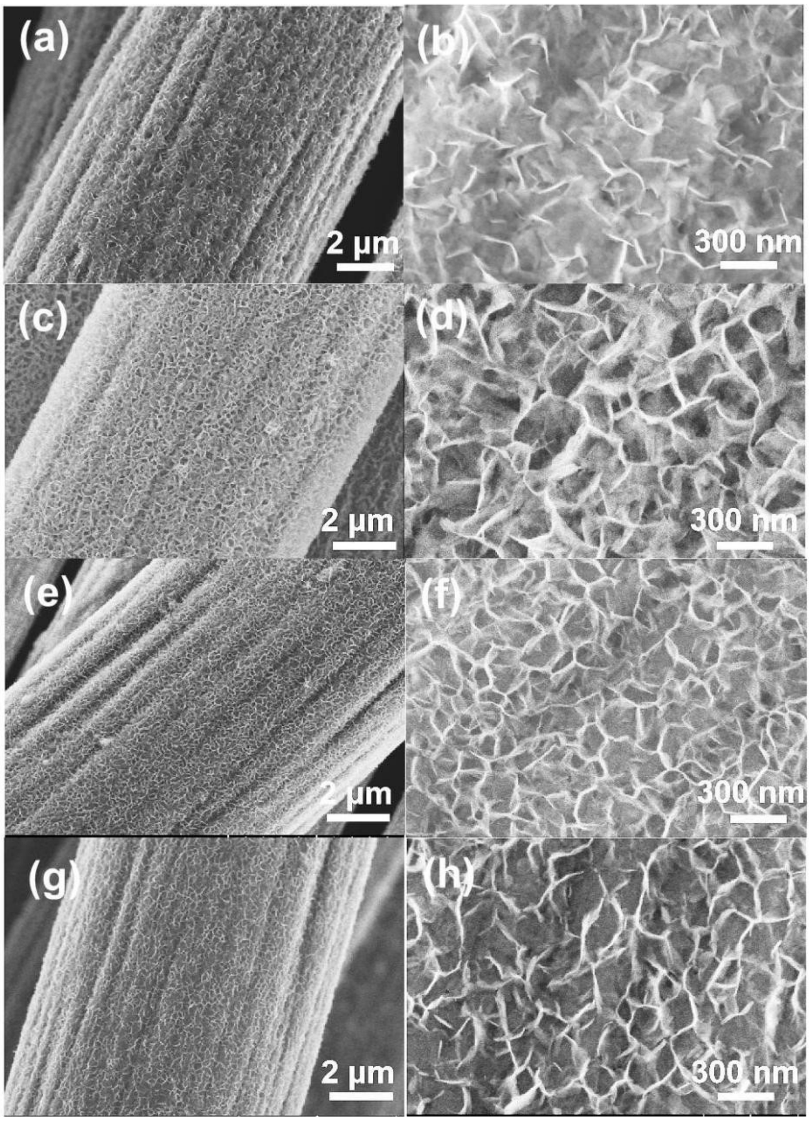

Fig.S4 SEM images of (a, b) β-$Ni(OH)_2$/CC, (c, d) FN MP/CC 4:10, (e, f) CFN MP/CC 1:4:10 and (g, h) CFN MP/CC 3:4:10.

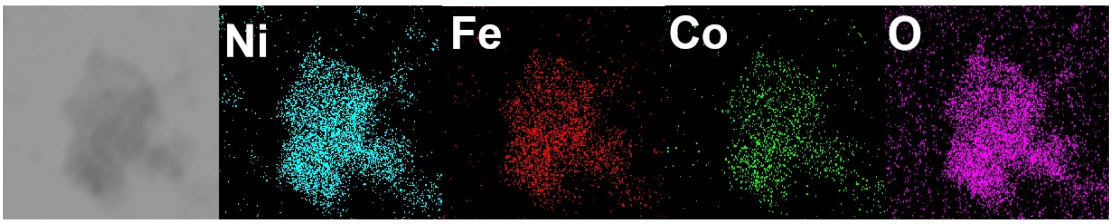

Fig.S5 EDS mapping of CFN MP/CC 2:4:10.

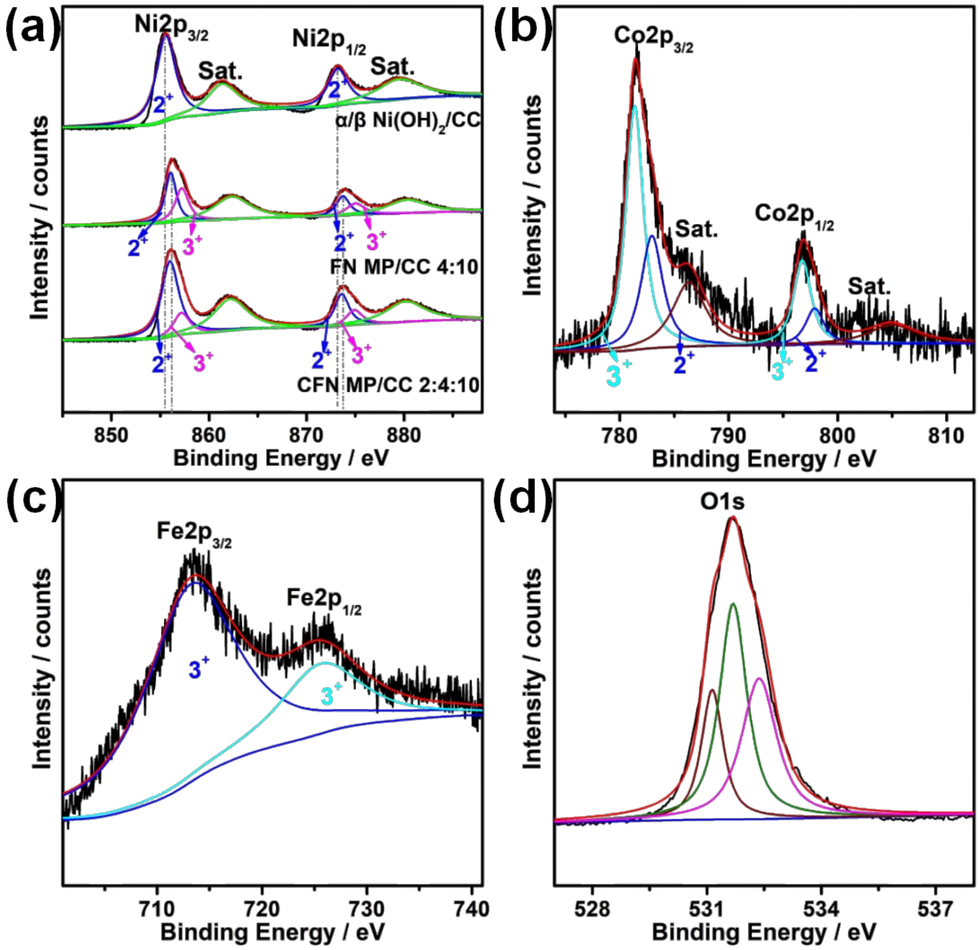

Fig.S6 High-solution XPS spectra of (a) Ni, (b) Co, (c) Fe and (d) O in the sample of CFN MP/CC 2:4:10.

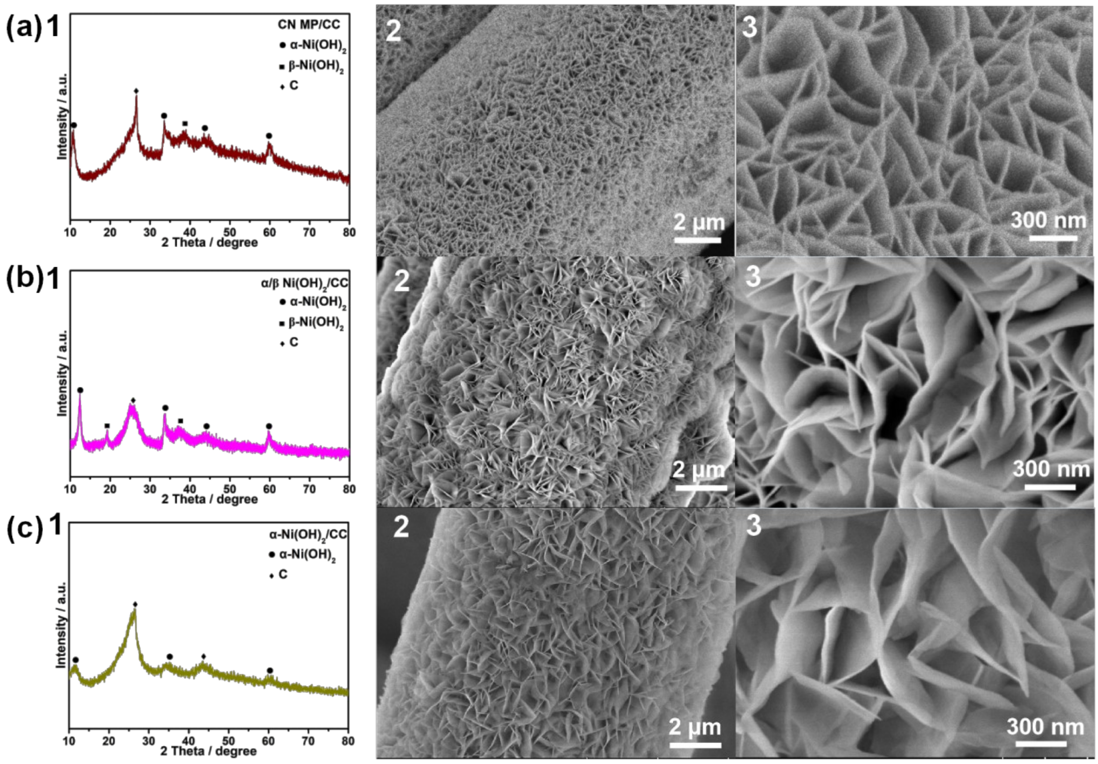

Fig.S7 Phase and morphological characterization of (a) CN MP/CC, (b) α/β $Ni(OH)_2$/CC and (c) α- $Ni(OH)_2$/CC: (1) XRD patterns, (2, 3) SEM images.

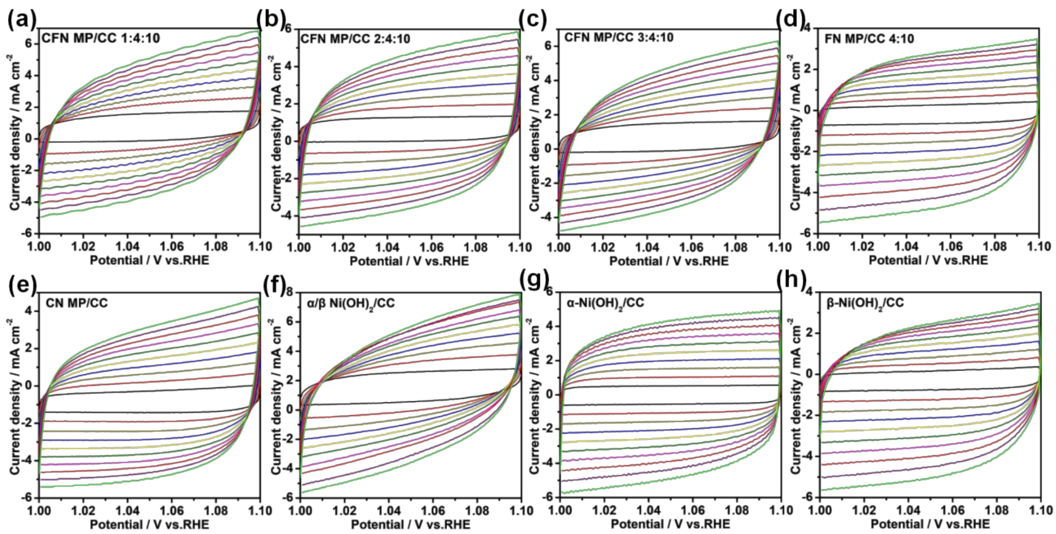

Fig.S8 CV curves of the samples at various scan rates from 10-100 mV s^{-1} in non-redox region.

The investigation of the electrochemical surface area (ECSA) of the samples was carried out according to literature.[1] ECSA was estimated by measuring the electrochemical double-layer capacitance. Cyclic voltammetry (CV) was employed at various scan rates from 10 to 100 mV s^{-1} in 1.0-1.1 V vs. RHE region, which could be considered as the double-layer capacitive behavior. The electrochemical double-layer capacitance (C_{dl}) can be calculated based on the CV curves (Fig.S8a-h). The value of C_{dl} is estimated by plotting the ΔJ (Ja-Jc) at 1.05 V vs. RHE against the scan rate, where the slope is twice C_{dl}.

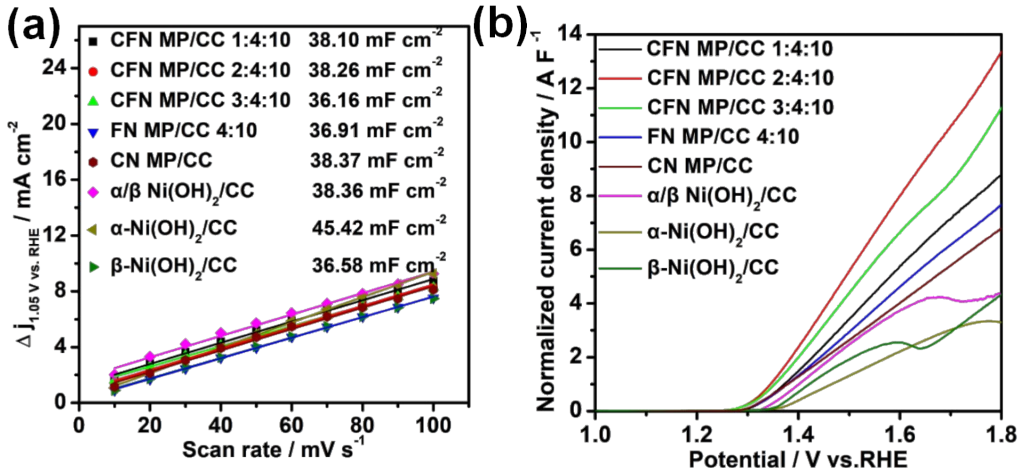

Fig.S9 (a) UOR current density variation at 1.05 V vs. RHE as a function of scan rate, (b) UOR LSV curves normalized by C_{dl}.

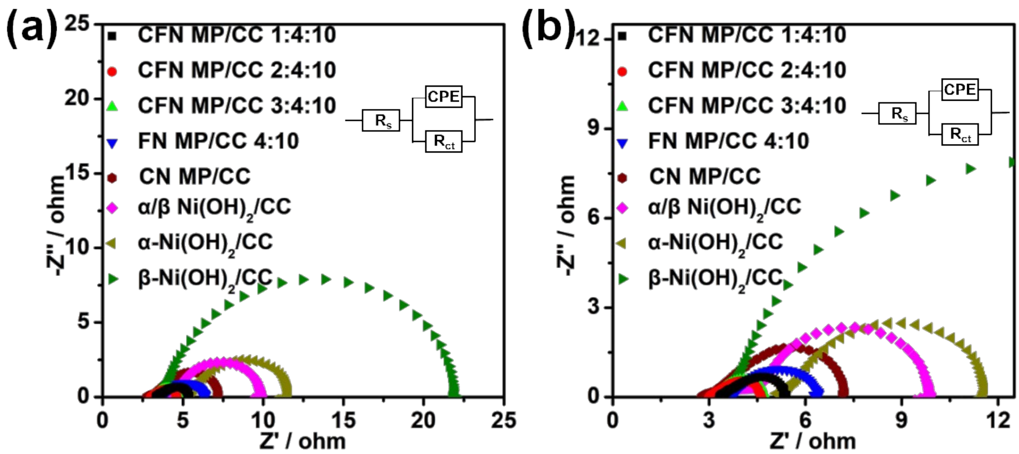

Fig.S10 (a) The EIS data of samples in 1 M KOH electrolyte and (b) the enlarged image (The insets in (a) and (b) are the equivalent circuit).

It can be seen from EIS spectra (Fig.S10 and Table S2) that the nickel hydroxide multiphase with only iron or cobalt incorporation displays lower values of R_s (series resistance) and R_{ct} (charge transfer resistance) than α/β $Ni(OH)_2$/CC, indicating that the addition of iron or cobalt can optimize the electronic structure of $Ni(OH)_2$ multiphase. Besides, cobalt, iron co-incorporated $Ni(OH)_2$ multiphase (CFN MP/CC) demonstrates lower R_s and R_{ct} than FN MP/CC and CN MP/CC, confirming that the Co-Fe-Ni polymetallic synergistic effect is stronger than the Fe-Ni bimetallic synergy on the modulation of the electronic structure of $Ni(OH)_2$ multiphase. But the remarkable thing is that different molar ratios of Co, Fe and Ni result in different levels of modulation on the electronic structure of $Ni(OH)_2$ multiphase. From Fig.S10 and Table S2, the sample of CFN MP/CC 2:4:10 possesses the lowest R_s (3.05 Ω) and R_{ct} (1.62 Ω), identifying the best electrical conductivity and the fastest electron transport rate owing to the regulation of iron and cobalt, thus displaying the highest catalytic activity for OER and UOR. However, CFN MP/CC 1:4:10 shows highest values of R_s (3.39 Ω) and R_{ct} (2.11 Ω) in CFN MP/CC samples, illustrating that this molar ratio has the weakest modulation effect on electronic structure, and thus revealing the worst catalytic performance. The conductivity and charge transfer rate of CFN MP/CC 3:4:10 were between the CFN MP/CC 1:4:10 and the CFN MP/CC 2:4:10, thus demonstrating the intermediate catalytic behavior. Therefore, the reason why the catalysts with different molar ratios of Co, Fe and Ni display diverse catalytic activity is the different modulation levels on the electronic structure of $Ni(OH)_2$ multiphase. And the optimal molar ratio of Co, Fe and Ni is 2:4:10 to achieve the catalytic activity optimization.

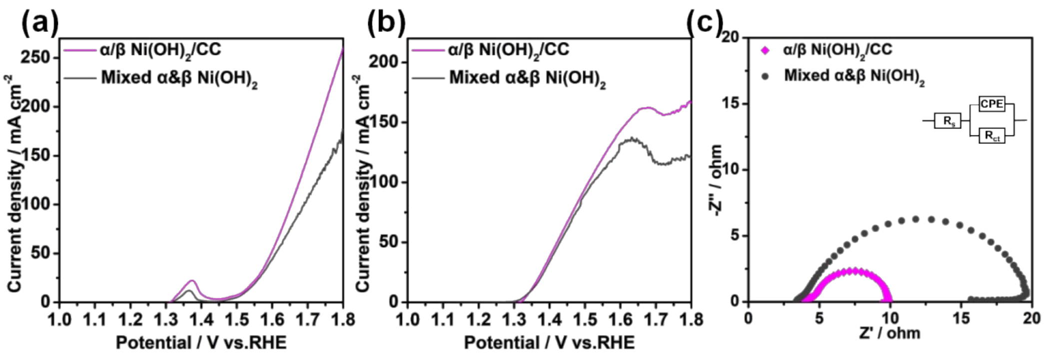

Fig.S11 Catalytic performance of mixed α-$Ni(OH)_2$ and β-$Ni(OH)_2$ powders: (a) LSV curves for OER, (b) LSV curves for UOR and (c) EIS data.

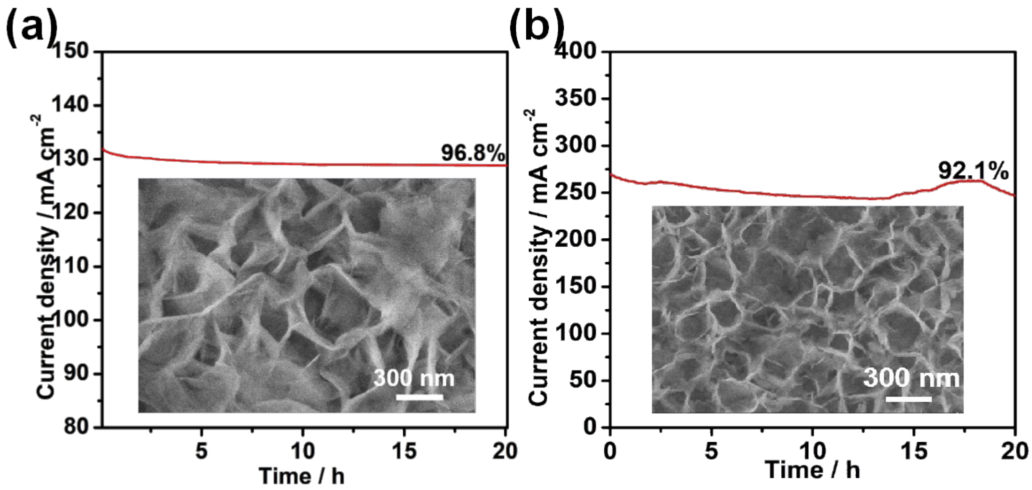

Fig.S12 Chronoamperometry test at 1.53 V vs. RHE for (a) OER and (b) UOR. The insets in (a) and (b) are the SEM images after stability test.

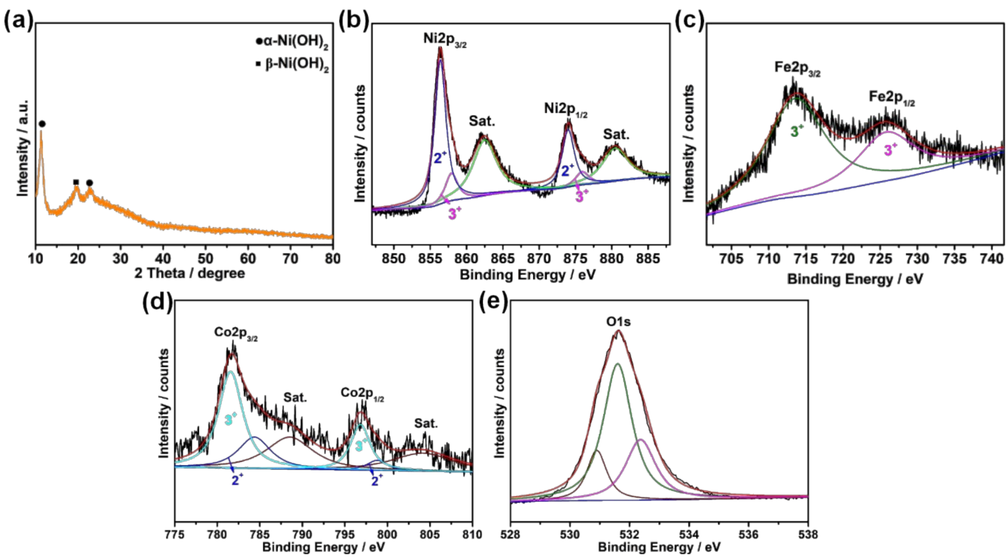

Fig.S13 XRD and high-solution XPS spectra of CFN MP/CC 2:4:10 after chronoamperometric test for OER: (a) XRD, (b) Ni, (c) Fe, (d) Co and (e) O.

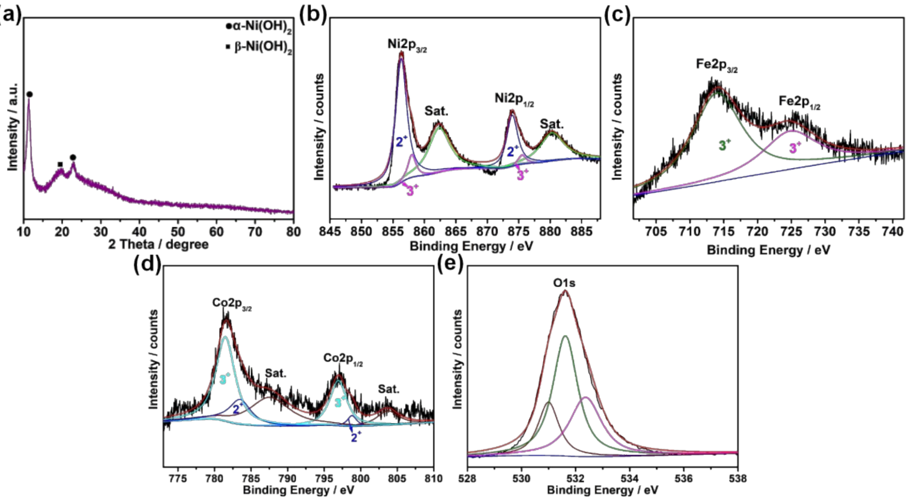

Fig.S14 XRD and high-solution XPS spectra of CFN MP/CC 2:4:10 after chronoamperometric test for UOR: (a) XRD, (b) Ni, (c) Fe, (d) Co and (e) O.

Table S1. Molar ratios of Co, Fe and Ni in the samples derived from the ICP analysis.

Sample	Molar ratio of Co, Fe and Ni
CFN MP/CC 1:4:10	0.86:2.73:10
CFN MP/CC 2:4:10	2.18:2.79:10
CFN MP/CC 3:4:10	2.96:2.87:10

Table S2. Comparison of electrocatalytic performance for OER and UOR

Samples	OER				UOR	
	Required potential for 10 mA cm^{-2} [V vs. RHE]	Tafel slope [mV dec^{-1}]	R_s[a] [Ω]	R_{ct}[b] [Ω]	Required potential for 10 mA cm^{-2} [V vs. RHE]	Tafel slope [mV dec^{-1}]
CFN MP/CC 1:4:10	1.437	66	3.39	2.11	1.321	60
CFN MP/CC 2:4:10	1.423	62	3.05	1.62	1.300	59
CFN MP/CC 3:4:10	1.436	64	3.11	1.69	1.304	69
FN MP/CC 4:10	1.446	83	3.70	2.81	1.322	73

CN MP/CC	1.433	140	3.21	4.22	1.321	75
α/β $Ni(OH)_2$/CC	1.515	95	4.57	5.38	1.347	59
α-$Ni(OH)_2$/CC	1.546	87	5.25	6.62	1.380	74
β-$Ni(OH)_2$/CC	1.561	173	3.57	18.77	1.368	61

[a] Series resistance. [b] Charge transfer resistance.

Table S3 Comparison of catalytic activity for OER on different reported catalysts.

Catalyst	Electrolyte	Current density at 1.53 V (mA cm^{-2})	Required potential at 10 mA cm^{-2} (V vs. RHE)	Reference
NiFe-LDH@CoS_x	1.0 M KOH	~75	1.436	Ref.[1]
CoP_2/Fe-CoP_2 YSBs	1.0 M KOH	~30	1.496	Ref.[2]
Ni-Co_3Se_4/rGO	1.0 M KOH	~15	1.514	Ref.[3]
FeS/Fe_3C@NS-C-900	0.1 M KOH	~20	1.500	Ref.[4]
Te/FeNiOOH-NCs	1.0 M KOH	~90	1.450	Ref.[5]
Ni-Fe-Se/CFP	1.0 M KOH	~30	1.511	Ref.[6]
NCN-CoMoS-700	1.0 M KOH	NA	1.463	Ref.[7]
N-NiVFeP/NFF	1.0 M KOH	~95	1.459	Ref.[8]
Fe_1Co_3/V_O-800	1.0 M KOH	~20	1.490	Ref.[9]
Re/ReS_2-7H/CC	1.0 M KOH	~15	1.520	Ref.[10]
Ni/$Ni_{0.2}Mo_{0.8}N$@N-C	1.0 M KOH	~25	1.490	Ref.[11]
NiFe-MOF-74/NF	1.0 M KOH	~100	1.438	Ref.[12]
p-$Cu_{1-x}NNi_{3-y}$/FeNiCu	1.0 M KOH	~15	1.490	Ref.[13]
$NiMn_2O_4$/rGO	1.0 M KOH	~25	1.514	Ref.[14]
Co/CNT/MCP-850	1.0 M KOH	~20	1.500	Ref.[15]
CFN MP/CC 2:4:10	1.0 M KOH	106	1.423	This work

Note: "~" stands for the estimated value from the LSV curves.

Table S4 Comparison of catalytic activity for UOR on different reported catalysts.

Catalyst	Electrolyte	Current density at 1.53 V (mA cm^{-2})	Required potential at 10 mA cm^{-2} (V vs. RHE)	Reference
N,S-doped carbon-$MnFe_2O_4$	1.0 M KOH with 0.5 M urea	~170	1.360	Ref.[16]
BSeFL/$Ni(OH)_2$ (-1.0 V)	1.0 M KOH with 0.5 M urea	~175	1.300	Ref.[17]
Ni-Bi	1.0 M KOH with 0.33 M urea	NA	1.350	Ref.[18]
NiCoP/CC	1.0 M KOH with 0.5 M urea	~90	1.300	Ref.[19]
Ni-MOF-0.5	1.0 M KOH with 0.5 M urea	~65	1.381	Ref.[20]
P-$CoS_x(OH)_y$ NN/Ti	1.0 M KOH with 0.5 M urea	~70	1.300	Ref.[21]
Ni_2P/Fe_2P/NF	1.0 M KOH with 0.5 M urea	~150	1.370	Ref.[22]
Ni_4N/Cu_3N/CF	1.0 M KOH with 0.5 M urea	~160	1.340	Ref.[23]
$Ni(OH)_2$@NF	1.0 M KOH with 0.3 M urea	NA	1.350	Ref.[24]
CoS_x/Co-MOF	1.0 M KOH with 0.5 M urea	~180	1.315	Ref.[25]
$NiCo_2S_4$ NS/Carbon cloth	1.0 M KOH with 0.33 M urea	~100	1.317	Ref.[26]
C@NiO	1.0 M KOH with 0.33 M urea	~175	1.360	Ref.[27]
NP-$Ni_{0.70}Fe_{0.30}$/NF	1.0 M KOH with 0.33 M urea	~200	1.330	Ref.[28]
CoFeCr LDH/NF	1.0 M KOH with 0.33 M urea	~225	1.305	Ref.[29]
CoP/C-3	1.0 M KOH with 0.10 M urea	~130	1.354	Ref.[30]
CFN MP/CC 2:4:10	1.0 M KOH with 0.33 M urea	231	1.300	This work

Note: "~" stands for the estimated value from the LSV curves.

Reference

[1] Y. Yang, Y. Xie, Z. Yu, S. Guo, M. Yuan, H. Yao, Z. Liang, Y. R. Lu, T.-S. Chan, C. Li, H. Dong and S. Ma, *Chem. Eng. J.* **2021**, *419*, 129512.

[2] V. Ganesan, J. Son and J. Kim, *Nanoscale* **2021**, *13*, 4569-4575.

[3] W. Ye, Y. Zhang, J. Fan, P. Shi, Y. Min and Q. Xu, *Nanoscale* **2021**, *13*, 3698-3708.

[4] Y. W. Li, W. J. Zhang, J. Li, H. Y. Ma, H. M. Du, D. C. Li, S. N. Wang, J. S. Zhao, J. M. Dou and L. Xu, *ACS Appl. Mater. Interfaces* **2020**, *12*, 44710-44719.

[5] S. Ibraheem, X. Li, S. S. A. Shah, T. Najam, G. Yasin, R. Iqbal, S. Hussain, W. Ding and F. Shahzad, *ACS Appl. Mater. Interfaces* **2021**, *13*, 10972-10978.

[6] Y. Guo, C. Zhang, J. Zhang, K. Dastafkan, K. Wang, C. Zhao and Z. Shi, *ACS Sustain. Chem. Eng.* **2021**, *9*, 2047-2056.

[7] M. Kim, H. Seok, N. Clament Sagaya Selvam, J. Cho, G. H. Choi, M. G. Nam, S. Kang, T. Kim and P. J. Yoo, *J. Power Sources* **2021**, *493*, 229688.

[8] H. Fan, W. Chen, G. Chen, J. Huang, C. Song, Y. Du, C. Li and K. Ostrikov, *Appl. Catal. B-Environ* **2020**, *268*, 118440.

[9] W. Chen, Y. Zhang, G. Chen, R. Huang, Y. Zhou, Y. Wu, Y. Hu and K. Ostrikov, *J. Mater. Chem. A* **2019**, *7*, 3090-3100.

[10] Q. Q. Pang, Z. L. Niu, S. S. Yi, S. Zhang, Z. Y. Liu and X. Z. Yue, *Small* **2020**, *16*, e2003007.

[11] T. Li, Y. Hu, X. Pan, J. Yin, Y. Li, Y. Wang, Y. Zhang, H. Sun and Y. Tang, *Chem. Eng. J.* **2020**, *392*, 124845.

[12] C. Chen, N. Suo, X. Han, X. He, Z. Dou, Z. Lin and L. Cui, *J. Alloys Compd.* **2021**, *865*, 158795.

[13] Y. Zhu, G. Chen, Y. Zhong, Y. Chen, N. Ma, W. Zhou and Z. Shao, *Nat. Commun.* **2018**, *9*, 2326.

[14] Q. Zhang, D. Liu, C. Zhang and Y. Tian, *Electrochim. Acta* **2018**, *280*, 266-277.

[15] X. Zhou, X. Liu, J. Zhang, C. Zhang, S. J. Yoo, J.-G. Kim, X. Chu, C. Song, P. Wang, Z. Zhao, D. Li, W. Zhang and W. Zheng, *Carbon* **2020**, *166*, 284-290.

[16] P. Balasubramanian, A. Jansirani, S.B. He, H.H. Deng, H.-P. Peng, X.-H. Xia and W. Chen, *J. Power Sources* **2021**, *494*, 229757.

[17] R. G. Jadhav and A. K. Das, *Nanoscale* **2020**, *12*, 23596-23606.

[18] J. Ge, Y. Lai, M. Guan, Y. Xiao, J. Kuang and C. Yang, *Environ. Sci. Nano* **2021**.

[19] L. Sha, J. Yin, K. Ye, G. Wang, K. Zhu, K. Cheng, J. Yan, G. Wang and D. Cao, *J. Mater. Chem. A* **2019**, *7*, 9078-9085.

[20] S. Zheng, Y. Zheng, H. Xue and H. Pang, *Chem. Eng. J.* **2020**, *395*, 125166.

[21] Y. Jiang, S. Gao, G. Xu and X. Song, *J. Mater. Chem. A* **2021**, *9*, 5664-5674.

[22] L. Yan, Y. Sun, E. Hu, J. Ning, Y. Zhong, Z. Zhang and Y. Hu, *J Colloid Interface Sci* **2019**, *541*, 279-286.

[23] J. Li, C. Yao, X. Kong, Z. Li, M. Jiang, F. Zhang and X. Lei, *ACS Sustain. Chem. Eng.* **2019**, *7*, 13278-13285.

[24] L. Xia, Y. Liao, Y. Qing, H. Xu, Z. Gao, W. Li and Y. Wu, *ACS Appl. Energy Mater.* **2020**, *3*, 2996-3004.

[25] H. Xu, K. Ye, K. Zhu, J. Yin, J. Yan, G. Wang and D. Cao, *Inorg. Chem. Front.* **2020**, *7*,

2602-2610.
[26] W. Zhu, M. Ren, N. Hu, W. Zhang, Z. Luo, R. Wang, J. Wang, L. Huang, Y. Suo and J. Wang, *ACS Sustain. Chem. Eng.* **2018**, *6*, 5011-5020.
[27] S. Lu, M. Hummel, Z. Gu, Y. Wang, K. Wang, R. Pathak, Y. Zhou, H. Jia, X. Qi, X. Zhao, B. B. Xu and X. Liu, *ACS Sustain. Chem. Eng.* **2021**, *9*, 1703-1713.
[28] Z. Cao, T. Zhou, X. Ma, Y. Shen, Q. Deng, W. Zhang and Y. Zhao, *ACS Sustain. Chem. Eng.* **2020**, 8, 11007-11015.
[29] Z. Wang, W. Liu, Y. Hu, M. Guan, L. Xu, H. Li, J. Bao and H. Li, *Appl. Catal. B-Environ* **2020**, *272*, 118959.
[30] J. Zheng, K. Wu, C. Lyu, X. Pan, X. Zhang, Y. Zhu, A. Wang, W.-M. Lau and N. Wang, *Appl. Surf. Sci.* **2020**, *506*, 144977.